Improved Assessment of the Flexibility Range of Distribution Grids Using Linear Optimization

Daniel A. Contreras, Krzysztof Rudion
IEH, University of Stuttgart
Stuttgart, Germany
daniel.contreras@ieh.uni-stuttgart.de

***Abstract*— Increasing use of flexible resources in electrical grids is forcing grid operators to intensify their cooperation to maintain grid stability. The contribution of this paper is the improvement of a method that allows the representation of the aggregated flexibility of distribution grids. The proposed model allows grid operators to show the status of their grid without needing to release sensitive grid data. To increase the precision of the model, linear models representing typical flexibility providers were developed. Then, an adaptation of the aggregation algorithm is introduced, based on linear optimization. The developed linear model has the objective to improve the computing time required by preceding nonlinear algorithms, while maintaining accuracy. The proposed model is validated using two real radial MV distribution grids in Germany. Results of the performed simulations show a considerable reduction of the required processing time, in grids with large amounts of flexible assets.**

***Index Terms*—Grid Flexibility, Flexibility Aggregation, TSO-DSO Coordination, Linear Optimization, Operation, Stability.**

I. INTRODUCTION

Distribution grids are evolving from their traditional passive character to an active one due to an enormous increase of distributed energy resources (DER) [1]. Consequently, the requirements for flexibilities to provide ancillary services to the grid (e.g. congestion management, voltage control) are expected to increase. In this paper, the term flexibility is defined as the "modification of generation or consumption in reaction to an external signal" [2]. This definition is extended reactive power as well. Within the ERA-Net project Callia, a market platform for transmission (TSO) and distribution system operators (DSO) is being developed, where flexibilities can be transacted to provide ancillary services to the grid. Using these flexibilities requires an improvement in the communication and coordination between system operators [3]. One example is Germany, where each TSO supplies more than one hundred DSOs within their control zones. This scenario makes it very difficult for any of the TSOs to achieve a proper level of coordination with all of their corresponding DSOs. Therefore, the improvement of the TSO-DSO coordination acquires a great relevance. In [4], a framework defining the roles and responsibilities for this purpose was proposed, as well as specific use cases for flexibilities. A similar approach is taken in [5], where five different TSO-DSO coordination schemes were developed and are currently being further researched.

A major issue is that grid operators are in many cases reluctant to share details of their grid models with other grid operators or market players. This may affect the coordination between them. Methods that allow them to communicate the status of the grid, without requiring the exposure of the grid topology, would be helpful. An aggregation approach to estimate the global flexibility of a distribution grid at the connection point to the transmission grid would help in this matter. The method allows grid operators to show the state of their grid, in terms of flexibility, without requiring sharing their grid topology. Additionally, it allows the evaluation of the effects in the grid caused by the application of specific flexible resources.

A methodology to estimate and aggregate the flexibility of a distribution grid at a given TSO-DSO interconnection point was first introduced in [6], based on Monte-Carlo simulations. The same authors drastically improved the methodology in [7] and [8], proposing the innovative nonlinear OPF-based Interval Constrained Power Flow (ICPF) algorithm. In [9] a variation of the aggregation algorithm is presented. The authors of [10] presented an alternative aggregation method using synthetic distribution grid feeders. The required processing time of the ICPF algorithm may be too large in some scenarios, requiring at least 15 minutes in some circumstances [8]. Such time-demanding solutions are not likely to be considered by grid operators within its everyday grid operation process. Consequently, this paper presents an improved approach to estimate the flexibility range of a distribution grid based on the concept proposed in [7]. The main objective is to reduce the computation time required by the algorithm to evaluate large grid models with plenty of flexible resources within a short period of time.

The paper is organized as follows: section II introduces linear models representing the technical limitations of typical flexible distribution grid resources. In section III, a linear optimization problem is formulated. Section IV presents the aggregation algorithm. Finally, in section V, the proposed

The research leading to this work is being carried out as part of the Callia Project "Open intra- and inter-DSO electricity markets for RES integration", http://callia.info, ERA-Net Smart Grids Plus. This project is supported by the Federal Ministry for Economic Affairs and Energy on the basis of a decision by the German Bundestag.

method is evaluated; using data from two real 20kV urban distribution grids, and is compared with the model of [7]. The paper closes with the conclusions and a brief outlook.

II. Modelling of Flexibility Providing Units (FPUs)

In this work, any decentralized generating unit, storage system or controllable load that can provide flexibility to an electrical grid is defined as a Flexibility Providing Unit (FPU). In both [7] and [8], the flexibility range of a FPU is represented through the rectangular limits of the active and reactive power flexibility (P_{flex} and Q_{flex}). This oversimplified representation neglects in many cases the dependency of active and reactive power limitations (e.g. *cos(φ)* limits or technical limits of inverters). To improve the representation of the operation range from typical grid utilities, five linear models are introduced in this work. These models intend to provide an accurate representation of the PQ flexibility range of each FPU. This allows obtaining more realistic aggregated flexibility ranges at the DSO-TSO interconnection point, while maintaining the linearity of the problem. The models intend to show the expected technical limits of the corresponding flexibilities, based on known technical parameters. It is possible to integrate other FPU models, based on measurements or different technologies, as long as they are represented by a convex polygon. This chapter defines five types of FPUs (Fig. 1).

A. Type 1

This model is the simplest representation of a FPU. It can be used to characterize FPUs with small flexible capability, as well as a simplification of a power inverter apparent power limit (in two- and four-quadrants operation modes). The model also represents storage systems or full converter wind generators ($P_B \geq 0$)). FPUs with no active power flexibility (e.g. STATCOMs) can be represented as well ($P_A = P_B = 0$) [11][12].

B. Type 2

A flexibility model with constant *cos(φ)* represents FPUs with linear dependence of active and reactive power, e.g. industrial loads with reactive power compensation [13].

C. Type 3

A representation of wind generators with DFIG, using rotor-side converters (RSC) with two-quadrant operation. At lower active power levels, the reactive power provision is possible, but limited by the inverter [12][15].

D. Type 4

Photovoltaic Generators can regulate their provision of reactive power through an inverter. This model allows to represent the compliance with *cos(φ)* specifications for PV (e.g. VDE 4105 [16]). In some cases, PV systems are required to help maintaining the voltage of the grid by modifying their power factor, using typical values of 0.9 or 0.95 (ind). A minimal plant operation level for generation units can be modelled as well, if necessary [14][17].

E. Type 5

Synchronous generators (SG) can be found in some DER, e.g. small hydro plants. This model represents an approximation of the operation chart of such generators. The apparent power limits of the SG are approximated linearly, as well as the stability limit. Minimal plant operation may be considered as well. [14][17]

III. Linear Optimization Model

The procedure presented in [7] formulates a nonlinear mixed-integer OPF problem to aggregate the flexibility range of a distribution grid at the DSO-TSO interconnection point (e.g. HV/MV transformer). The procedure aggregates the convex polygons delimiting the PQ boundaries of every FPU within the distribution grid. The result is a convex polygon representing the overall flexibility of the grid. In Fig. 2, an illustration of this process is shown. The crosses represent the expected operation point of the FPUs and the distribution grid (from the grid side) at a given moment. Grid constraints (i.e. voltage and branch flow limits) are considered in the optimization. The aggregated flexibility range (area at slack node in Fig. 2) takes into account the grid state and corresponds to only such operation points, where no voltage band violations or overloaded power lines are present.

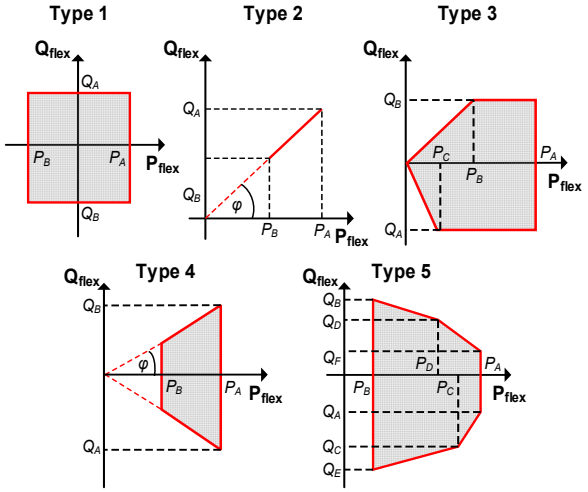

Figure 1. Definition of the flexibility boundaries of five types of FPUs

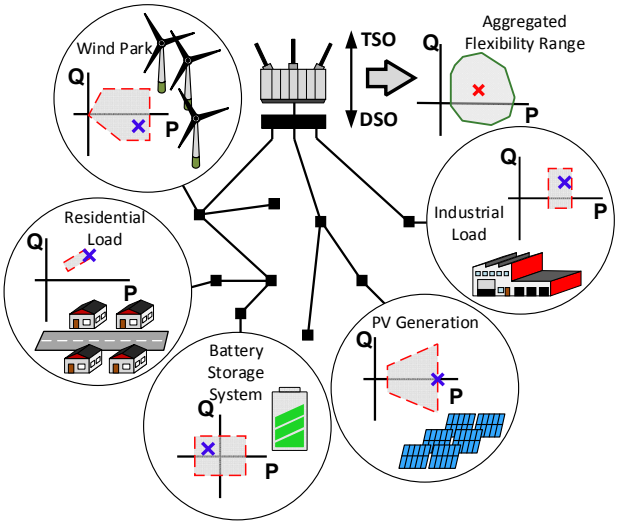

Figure 2. Representation of the aggregation of flexibility boundaries.

The nonlinear power flow equations accurately represent the status of a power grid, but at high computational cost in case of larger grids. The objective of this paper is to provide a method that allows reducing the computational burden required to aggregate the flexibility of grids with a manifold of FPUs. This chapter introduces a linear OPF model, constrained by the polygonal boundaries of FPUs, the node voltage limits and the linearized branch flow limits. The objective function performs the aggregation of the FPU boundary polygons in one particular direction within a PQ Cartesian space.

A. Linearization of Power Flow Nodal Equations

The power flow equations in polar coordinates are nonlinear, with voltages u and angles θ tightly coupled:

$$P_i(u,\theta) = u_i \cdot \sum_{j=1}^{n} Y_{ij} \cdot u_j \cdot cos\left(\theta_i - \theta_j - \alpha_{ij}\right) \quad (1)$$

$$Q_i(u,\theta) = u_i \cdot \sum_{j=1}^{n} Y_{ij} \cdot u_j \cdot sin\left(\theta_i - \theta_j - \alpha_{ij}\right) \quad (2)$$

The nodal balance equations (3) and (4) consider all generators and loads connected to node i, divided into fixed and flexible parts. The fix part is the expected operation point of non-flexible utilities, while the flex part is the flexibility provided by the FPUs (generators G, loads L and storage systems S). Active and reactive power flexibility provided by FPUs are added to Eqs. (3) and (4) as variables P_{flex} and Q_{flex}:

$$\Delta P_i = \sum_F \left(P_{fix,F,i} + P_{flex,F,i}\right) - P_i(u,\theta), F \in \{G \cup L \cup S\} \quad (3)$$

$$\Delta Q_i = \sum_F \left(Q_{fix,F,i} + Q_{flex,F,i}\right) - Q_i(u,\theta), F \in \{G \cup L \cup S\} \quad (4)$$

The power flow equations in polar coordinates, for a grid with n nodes and m FPUs, requires $2n + 2m$ decision variables (u, θ for each bus and P_{flex}, Q_{flex} for each FPU). The voltage at the slack node is preserved constant at 1 p.u and angle 0°. The traditional Newton-Raphson power flow (NR-PF) algorithm iteratively linearizes grid equations (1) and (2) using first order Taylor expansion. The algorithm optimizes u and θ on each iteration, by minimizing ΔP_i and ΔQ_i in (3) and (4), until they are within a defined tolerance limit. Iteration k of the NR-PF can be written, in terms of the Jacobian matrix J_k, as follows:

$$\begin{bmatrix}\Delta\theta_i \\ \Delta u_i\end{bmatrix}_{k+1} = \begin{bmatrix}\frac{\partial P_i}{\partial\theta} & \frac{\partial P_i}{\partial u} \\ \frac{\partial Q_i}{\partial\theta} & \frac{\partial Q_i}{\partial u}\end{bmatrix}_k^{-1} \cdot \begin{bmatrix}\Delta P_i \\ \Delta Q_i\end{bmatrix}_{k+1} = J_k^{-1} \cdot \begin{bmatrix}\Delta P_i \\ \Delta Q_i\end{bmatrix}_{k+1} \quad (5)$$

The Jacobian J_k is updated on each iteration using the corrected values of u and θ, and its inverse J_k^{-1} is calculated (Eq. (5)). The search direction of the optimization problem is adjusted until convergence is achieved. The NR-PF algorithm shows a very fast convergence in properly defined grids, requiring in most cases very few iterations to converge. Traditionally, a flat-start (u = 1 p.u., θ = 0° for all nodes) proves to be a good initial guess for the NR-PF algorithm. Providing an initial guess closer to the operation point of the grid would help the algorithm to converge even faster. This characteristic of the NR-PF is exploited here to linearize the power flow equations [18]. The state vector x of the linear OPF contains variables u, θ, P_{flex} and Q_{flex}. The initial state vector x_0 is obtained through a standard NR-PF of the selected grid with P_{flex} and Q_{flex} set to zero for all FPUs, thus resulting in the initial values for u and θ. Once the NR-PF algorithm converges, after $k = n$ iterations, the inverse of the Jacobian $J_{x0} = J_n$ can be used as the linearization constant for the linear model (Eq. (6)). The resulting linear grid model is expressed in terms of the state vector x as:

$$\begin{bmatrix}\Delta\theta_i \\ \Delta u_i\end{bmatrix}_x = \begin{bmatrix}\theta_i \\ u_i\end{bmatrix}_x - \begin{bmatrix}\theta_i \\ u_i\end{bmatrix}_{x_0} = J_{x_0}^{-1} \cdot \begin{bmatrix}\Delta P_i \\ \Delta Q_i\end{bmatrix}_x \quad (6)$$

Any modification to P_{flex} and Q_{flex} has a direct influence on u and θ. This causes state vector x to drift around the initial state vector x_0. Therefore, the error of linearizing the grid model around x_0 is expected to be smaller than when a flat-start is used as the linearization point. Finally, the magnitude of the nodal voltages u are constrained to:

$$u_{i,min} \le u_i \le u_{i,max} \quad (7)$$

Eqs. (1) and (2) directly relate to the grid topology through the admittance matrix Y, so does the Jacobian J_{x0}. Operating an OLTC transformer modifies Y according to the tap position, thus altering J_{x0} and its inverse. Consequently, the tap position cannot be considered as an independent decision variable, as was the case in [7]. For each tap position, both matrixes Y and J_{x0} need to be recalculated, thus forcing to determine independent flexibility areas for each tap position. This statement applies to changes in the grid topology as well.

B. Linearization of Branch Flow Constraints

Branch flows are limited by the maximal apparent power of each branch. This is formulated as a quadratic equation:

$$\sqrt{P_{ij}^2 + Q_{ij}^2} \le S_{ij,max} \quad (8)$$

A linear OPF model requires linear branch flow constraints. According to [19] and [20], Eq. (8) can be approximated through regular polygons of n sides, without compromising the numerical stability of the optimization problem. The apparent power limit of a branch is then approximated piecewise by n segments $L_{ij,k}$ (red dotted lines in Fig. 3, $k = 1,\ldots,n$). This means that n linear inequalities $L_{ij,k}$ per branch are required. Eq. (9) shows a straight line equation, defining each segment $L_{ij,k}$, shown in Fig. 3, where parameters a, b and c depend on angle α and the maximal branch flow $S_{ij,max}$.

$$L_{ij,k} = a_{ij,k} \cdot P_{ij} + b_{ij,k} \cdot Q_{ij} + c_{ij,k} \le 0, \forall k = 1,\ldots,n \quad (9)$$

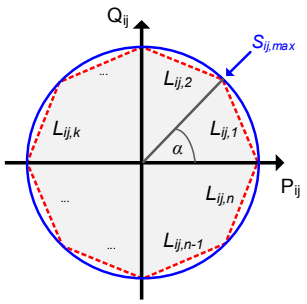

Figure 3. Piecewise linearization of the branch flow constraints. [20]

The active and reactive power flow through the branch connecting nodes i and j, is defined as:

$$P_{ij}(u,\theta) = u_i \cdot Y_{ij} \cdot \left(u_i \cdot cos(\alpha_{ij}) - u_j \cdot cos(\theta_i - \theta_j - \alpha_{ij})\right) \quad (10)$$

$$Q_{ij}(u,\theta) = u_i \cdot Y_{ij} \cdot \left(u_i \cdot sin(-\alpha_{ij}) - u_j \cdot sin(\theta_i - \theta_j - \alpha_{ij})\right) \quad (11)$$

The linearization of Eqs. (10) and (11) follows a similar procedure than with Eqs. (1) and (2), based on the extended Jacobian used for state estimation problems. The constant Jacobian for P_{ij} and Q_{ij} is obtained from the partial derivatives of Eqs. (10) and (11), evaluated in the initial state vector x_0 already obtained from Eq. (6). The linearized branch flow equations are defined in terms of the state vector x as follows:

$$\begin{bmatrix}\Delta P_{ij}\\ \Delta Q_{ij}\end{bmatrix}_x = \begin{bmatrix}\Delta P_{ij}\\ \Delta Q_{ij}\end{bmatrix}_{x_0} + \begin{bmatrix}\frac{\partial P_{ij}}{\partial \theta} & \frac{\partial P_{ij}}{\partial u}\\ \frac{\partial Q_{ij}}{\partial \theta} & \frac{\partial Q_{ij}}{\partial u}\end{bmatrix}_{x_0} \cdot \begin{bmatrix}\Delta \theta_i\\ \Delta u_i\end{bmatrix}_x \quad (12)$$

A system of equations linking the branch flows with state variables u and θ is obtained (Eq. (12)). Although a flat-start initialization is easier to implement, linearizing around the operation point x_0 improves the precision. Integrating Eqs. (9) and (12), a system of linear inequalities is obtained, which constrains the apparent power S_{ij} of each branch (Eq. (13)). These equations depend directly on state variables u and θ:

$$\left(a_{ij,k}\frac{\partial P_{ij}}{\partial \theta_i}\Big|_{x_0} + b_{ij,k}\frac{\partial Q_{ij}}{\partial \theta_i}\Big|_{x_0}\right)\Delta\theta_i + \left(a_{ij,k}\frac{\partial P_{ij}}{\partial \theta_j}\Big|_{x_0} + b_{ij,k}\frac{\partial Q_{ij}}{\partial \theta_j}\Big|_{x_0}\right)\Delta\theta_j +$$
$$\left(a_{ij,k}\frac{\partial P_{ij}}{\partial u_i}\Big|_{x_0} + b_{ij,k}\frac{\partial Q_{ij}}{\partial u_i}\Big|_{x_0}\right)\Delta u_i + \left(a_{ij,k}\frac{\partial P_{ij}}{\partial u_j}\Big|_{x_0} + b_{ij,k}\frac{\partial Q_{ij}}{\partial u_j}\Big|_{x_0}\right)\Delta u_j +$$
$$a_{ij,k} \cdot P_{ij,x_0} + b_{ij,k} \cdot Q_{ij,x_0} + c_{ij,k} \le 0 \quad (13)$$

C. Linear FPU constraints

The flexibility boundaries of five different types of FPUs, in a Cartesian PQ plane, were defined in the previous chapter. The boundaries of the FPUs are modelled as straight lines, represented by Eq. (14). These equations constraint the state variables P_{flex} and Q_{flex}. Parameters $a_{flex,i,t}$, $b_{flex,i,t}$ and $c_{flex,i,t}$ define the segments t of the convex polygons defining each FPU connected to node i (from Fig. 1). Each FPU type requires a different amount of line equations, depending on the number of sides each polygon has. Following this definition, a convex linear inequalities system is obtained for the FPUs, in the following form:

$$a_{flex,i,t} \cdot P_{flex,i} + b_{flex,i,t} \cdot Q_{flex,i} + c_{flex,i,t} \le 0 \quad (14)$$

D. Definition of Constrained Linear OPF

The proposed linear optimization method is formulated as a minimization problem using MATLAB's function '*linprog*':

$$\min f^T \cdot x \; subject\; to \begin{cases} A_{eq} \cdot x = b_{eq} & Eq.(6) \\ A \cdot x \le b & Eq.(13),(14) \\ lb \le x \le ub & Eq.(7) \end{cases} \quad (15)$$

Where vector x contains state variables u, θ, P_{flex}, *and* Q_{flex}. Parameters A_{eq} and A are matrixes, while b_{eq}, b, lb and ub are vectors. Vector f^T defines the objective function, a line equation in a PQ Cartesian space that represents the active and reactive power exchange through the slack node from or towards an over layered grid (i.e. through a MV/HV transformer). The model assumes grids with just one outside connection, thus only one slack bus [7]. The complex branch flow $S_{slack,x} = P_{slack,x} + jQ_{slack,x}$ is defined as the power flow coming from the slack bus into the grid (based on Eq. (12)). The flexibility range of the grid is then defined by pairs of points ($P_{slack,x}$, $Q_{slack,x}$) computed using the following objective function:

$$f^T = \gamma \cdot \left(P_{slack,x} + \beta \cdot Q_{slack,x}\right) \quad (16)$$

Maximizing or minimizing Eq. (16) allows finding different boundary points ($P_{slack,x}$, $Q_{slack,x}$) of the aggregated flexibility range of the grid in defined directions of the PQ Cartesian plane. Parameter γ can be set to -1 or 1, defining a maximization or minimization optimization problem, while β defines the direction in which the boundary points are scanned. This allows the exploration in all 360° from the grid operation point ($P_{slack,x0}$, $Q_{slack,x0}$). The next chapter details how the aggregated flexibility range of a distribution grid is obtained with Eq. (16).

IV. Distribution Grid Flexibility Range Estimation

The methodology to determine the flexibility range of a distribution grid has basis on the ICPF algorithm proposed in [7]. The objective is to determine the range of all feasible solutions for the exchanged power flow from and to the over layered grid through the slack node, by aggregating the flexibility ranges of all FPUs within the distribution grid. Every solution is required to satisfy all grid voltage and line loading constraints. The search algorithm assumes a convex solution space, since all FPUs limits are defined as convex polygons, so are the grid constraint. The algorithm requires to know the technical limits of every FPU (based on Fig. 1), including the connection point and if they are operating or not at the moment. The quality of the observability of the operation point of the FPUs has a direct influence in the quality of the linearization of the grid model. Linearizing from the grid operation point, instead of a flat-start, improves the quality of the linearization. A full knowledge of the grid topology is expected as well. A flowchart of the proposed algorithm can be seen in Fig. 4.

The search procedure begins with the exploration of the extreme boundary points P_{max}, P_{min}, Q_{max} and Q_{min}, by minimizing or maximizing Eq. (16) with β initially selected as 0 or ∞, respectively (red points in Fig. 5). The intersection of the straight lines connecting the boundary points P_{min} - P_{max} and Q_{min} - Q_{max} defines four search quadrants (areas I-IV in Fig. 5). After this point, β becomes a variable and is defined as the slope of the straight lines connecting adjacent boundary points (red dotted lines in Fig. 5). Within a quadrant, all β have the same sign. Table I shows the expected sign of variable β and the value of parameter γ to be used in Eq. (16) on each defined quadrant.

TABLE I. Objective Function Components by Quadrant

Quadrant	*I*	*II*	*III*	*IV*
sign(β)	-	+	-	+
γ (Eq. (17))	1	-1	-1	1

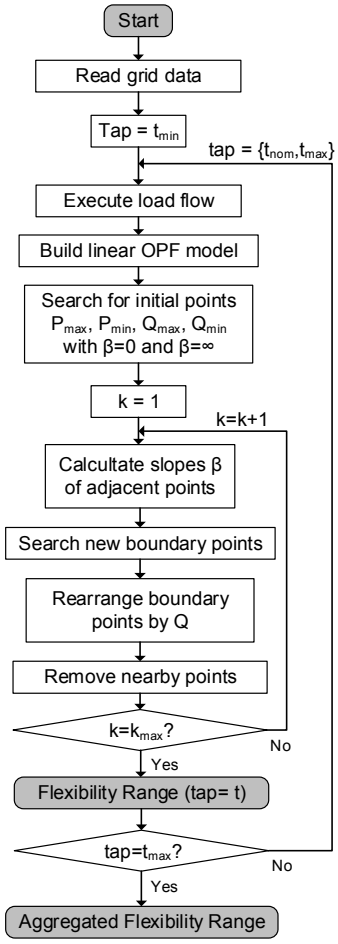

Figure 4. Flow chart of the linear flexibility range aggregation algorithm.

Having computed the first set of β (red dotted lines in Fig. 5), the iterative exploration of the quadrants is then initiated (green triangles in Fig. 5). All four quadrants can be explored independently and in parallel. For each iteration, the obtained boundary points in all quadrants are reorganized by reactive power value (from higher to lower). Points located too close to each other, within a predefined range ε, are discarded. Subsequent iterations repeat the search process using new values of β, calculated from the new sets of boundary points (e.g. blue squares in Fig. 5). The process stops after k_{max} iterations.

In [7], the search algorithm converges when the angle difference (ϕ) between all adjacent segments is below a predefined threshold. This allows obtaining a smooth contour, but the algorithm may not converge if the solution space has sharp corners. In this work, the maximal amount of iterations is predefined, in order to maintain a constant processing time and to disallow unnecessary iterations. After k iterations, a maximal amount of 2^{k+2} contour points is obtained (2^k-1 for each quadrant). It was observed that $k = 3$ iterations are sufficient to obtain a representative approximation of the aggregated flexibility range (max. 2^5 boundary points). The resulting contour is the convex hull defined by the boundary points after the last iteration (e.g. blue lines in Fig. 5).

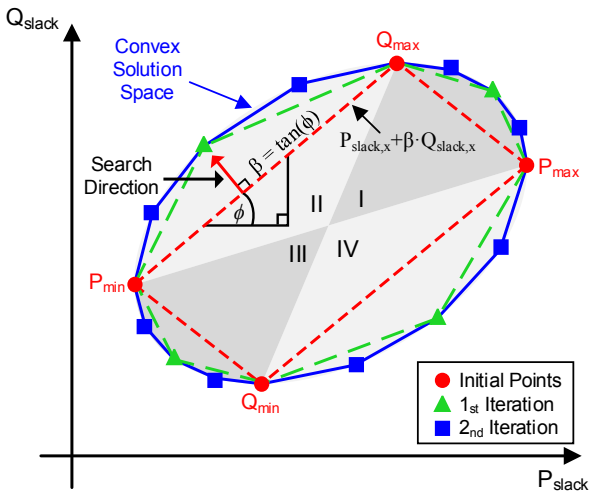

Figure 5. Representation of the search procedure.

The consideration of the tap changer as a flexibility, forces the search process to be repeated independently for each tap position. Changing the tap position directly alters the impedance and voltage profile of the grid, affecting the reactive power flexibility (shift of the aggregated flexibility among the Q-Axis in Fig. 6). The resulting aggregated flexibility of the grid results from the union of the flexibility areas obtained for all tap positions. The tap changer has very little effect over the active power flexibility, allowing the algorithm to be optimized by considering only the nominal and extreme positions of the tap. At one end, only quadrants I and II need to be explored, while quadrants III and IV are required at the other end. The nominal tap flexibility area is required to ensure a correct determination of the active power limits.

V. Case Study

In this section, the proposed method is verified in two real 20kV urban distribution grid feeders from Heidelberg, Germany. The grids are labelled as Grid A (75 Nodes) and Grid B (110 Nodes). Both are operated as open rings and are fed through 110/20 kV OLTCs (Fig. 7). Generation and load characteristics of the grids are detailed in Table II. To test the effectiveness of the algorithm, every load and generator in the grids is considered as a FPU. No storage systems are available. The distribution of the FPUs in the grids is found in Table III.

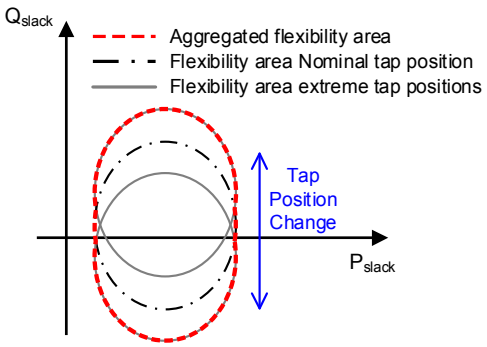

Figure 6. Effect of the tap changer in the solution space.

Simulations were performed using MATLAB on a laptop with an i5-6300U 2.4GHz processor, 8GB RAM and a 64 Bits Windows 10 operating system. Voltage limits were set to 0.9 p.u. and 1.1 p.u for all nodes. Simulations consider cases with and without OLTCs as flexibility. Transformers on both grids consider maximal tap positions of ±4%, with 1% change per step. The branch flows limits (Eq. (13)) were approximated using n = 8 linear equations. The proposed algorithm was tested using a 'Simplex' solver without any parallelization of the search procedure.

A. Results for Grid A

The first scenario considers a medium sized grid with high levels of self-consumption. Most flexibility is obtained by the curtailment of generation units, and load shedding. All loads are allowed to reduce its consumption by maximum 10% (Type 2 models). Results show that the flexibility areas obtained using the proposed linear-model is almost identical to the area obtained using the ICPF nonlinear model, modified to include the defined FPU models (Fig. 8). The obtained boundary points were validated with a NR-PF calculation. The average difference between the results obtained from the linear model and from the NR-PF are 24 kW and 67 kVAr for all points (average relative errors of 0,31% and 5,97% respectively). Selecting a proper linearization point proves then to be very important. Linearizing around a flat-start (magenta dotted line in Fig. 8) caused a larger deviation of the flexibility area compared to the one obtained by linearizing around the grid operation point x_0 (red line in Fig. 8). The linearization error increases when the distance between the boundary point $P_{slack,x}$ and the grid operation point $P_{slack,x0}$ increases. For this scenario, although the ICPF algorithm proves to be effective, the proposed model produces results of the same quality, while reducing the computation time in 80%. The results are summarized in Table IV.

TABLE II. DISTRIBUTION GRIDS PARAMETERS

Parameter	Grid A		Grid B	
	MW	*MVAr*	*MW*	*MVAr*
Total Load	10,85	3,54	17,22	5,65
Total Generation	7,59	0	7,21	0
Grid Losses	0,045	0,07	0,022	0,22
Branch Reactive Charging	0	-1,5	0	-1,9
Grid Operation Point	3,28	2,10	10,03	3,94

TABLE III. DISTRIBUTION OF FPU TYPES IN STUDIED GRID MODELS

Grid	Total FPUs	FPU Type				
		1	*2*	*3*	*4*	*5*
Grid A	79	0	70	4	3	2
Grid B	130	0	101	15	7	7

B. Results for Grid B

The second tested scenario considers a larger grid with large amounts of FPUs (130 in total). The proposed aggregation model is able to provide an accurate aggregation, reducing the computation time in 97,76% compared to the ICPF algorithm. The obtained boundary points were confirmed with a NR-PF calculation, showing an average difference of 3 kW and 31 kVAr (representing an average relative error of 0,02% and 11,3% respectively). The linearized model provides a result of good quality, as long as the aggregated area remains close to the grid operation point. For the ICPF algorithm, this scenario showed some of its limitations, as the algorithm could not converge at every expected boundary point, reducing the obtained flexibility area. The search procedure may miss an entire section if one boundary point is not correctly located, as can be observed in Fig. 9. A summary of the results is shown in Table IV.

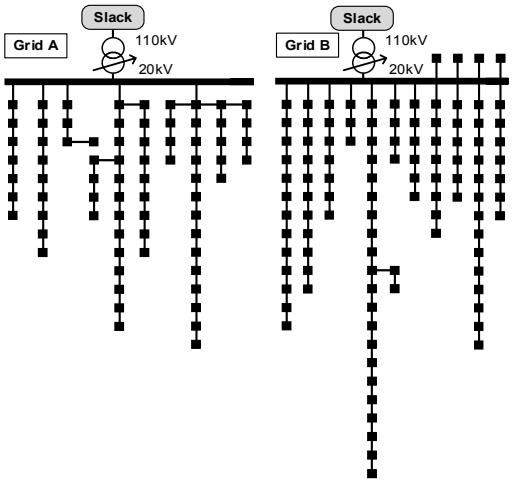

Figure 7. 75 nodes (Grid A) and 110 Nodes (Grid B) 20 kV test grids.

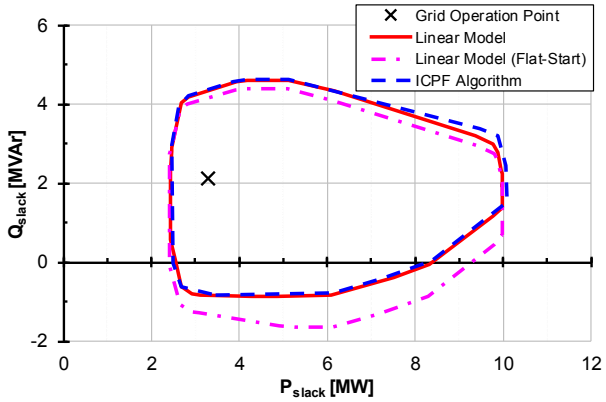

Figure 8. Aggregated flexibility for Grid A considering tap-changer.

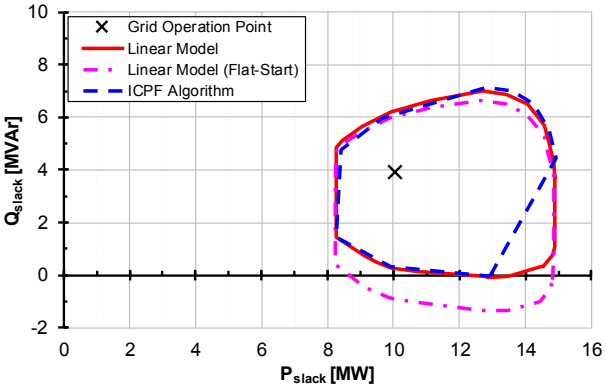

Figure 9. Aggregated flexibility for Grid B considering tap-changer.

TABLE IV. SUMMARY OF RESULTS OF SIMULATIONS

Parameter		Model	Grid A	Grid B
Flex Area Size (MVA^2)	***With Tap***	*Linear*	32,24	39,76
		Nonlinear	33,45	35,33
	Without Tap	*Linear*	31,34	38,49
		Nonlinear	31,50	35,56
Time (s)	***With Tap***	*Linear*	43	120
		Nonlinear	199	5365
	Without Tap	*Linear*	17	53
		Nonlinear	153	3061

VI. CONCLUSIONS

In this paper, a linear optimization model for the aggregation of active and reactive power flexibility of distribution grids at a TSO-DSO interconnection point was presented. The power flow equations were linearized by using the Jacobian matrix of the Newton-Raphson algorithm in a smart way. The model was complemented with non-rectangular linear representations of typical FPUs, increasing the accuracy of the distribution grid aggregation. The obtained linear programming system allows a considerable reduction of the required computing time for the process. At the same time, it maintains the accuracy of the power flow calculations and increases the stability of the search algorithm while considering large grid models.

The algorithm was tested in two different radial urban distribution grids in Germany, in scenarios with high quantity of FPUs. The model was implemented using linear programming tools in MATLAB. Comparisons with the ICPF algorithm of [7] show a remarkable improvement of the computation time, while the obtained solution deviates very little from the nonlinear model. In a scenario with more than hundred FPUs, the proposed model shows its fortitudes, requiring just less than 3% of the computing time than the original nonlinear model in the case of the largest tested grid. The quality of the solution shows very little variation from the nonlinear model. This variation of the algorithm is promising and has the potential to be further developed and improved, offering an effective tool to advance in the study of the utilization of flexibilities in distribution grids.

The developed method can have many practical applications, which could improve the coordination between grid operators. It can help evaluate the effect of the activation of flexibilities by TSOs located within DSO grids (e.g. for frequency control purposes). The impact of flexibility markets could be observed by including market results as constraints in the OPF model. Distribution grids operating at more than a one high voltage level can be represented by the aggregation of the results acquired from the single feeders, therefore reducing the need to declare sensitive grid information. Characteristics, which are being researched within the Callia project.

ACKNOWLEDGMENT

The authors would like to thank the German Federal Ministry for Economic Affairs and Energy for the support of the Callia Project, as well as the Stadtwerke Heidelberg Netze GmbH for its cooperation, and B. Wagner for his contributions.

REFERENCES

[1] S. Ruester, S. Schwenmen, C. Batlle, and I. Pérez-Arriaga, „From Distribution Networks to Smart Distribution Systems: Rethinking the Regulation of European Electricity DSOs," in *Utilities Policy*, Vol. 31, pp. 229-237, Apr. 2014.

[2] EURELECTRIC, "Active Distribution System Management" [Online], Feb. 2013. Available: http://www.eurelectric.org/media/74356/asm_full_report_discussion_paper_final-2013-030-0117-01-e.pdf

[3] EDSO, "Flexibility: The role of DSOs in tomorrow's electricity market" [Online], 2014. Available: http://www.edsoforsmartgrids.eu/wp-content/uploads/public/EDSO-views-on-Flexibility-FINAL-May-5th-2014.pdf

[4] ENTSO-E, CEDEC, GEODE, EURELECTRIC, and EDSO for Smart Grids, "TSO-DSO Data Management Report," [Online], Jul. 2016. Available: http://www.eurelectric.org/media/285585/tso-dso_dm_rep-2016-030-0382-01-e.pdf

[5] H. Gerard, E. Rivero, and D. Six, "Basic models for TSO-DSO coordination and ancillary services provision," EC Horizon 2020 Project SmartNet [Online], GNo 691405, SmartNetD1.3, 2016. Available: http://smartnet-project.eu/wp-content/uploads/2016/12/D1.3_20161202_V1.0.pdf

[6] M. Heleno, et al. "Estimation of the Flexibility Range in the Transmission-Distribution Boundary," in *IEEE PowerTech*, Eindhoven, Netherlands, June 2015.

[7] J. Silva et al., "Estimating the Active and Reactive Power Flexibility Area at the TSO-DSO Interface," in IEEE Transactions on Power Systems, 2018.

[8] N. Fonseca, et al., "EvolvDSO Grid Management Tools to Support TSO-DSO Cooperation," in *CIRED*, Helsinki, Finland, June 2016.

[9] H. Chen and A. Moser, "Improved flexibility of active distribution grid by remote control of renewable energy sources," in *International Conference on Clean Electrical Power*, Liguria, Italy, Jun. 2017.

[10] G. Petretto, et al., "Representative Distribution Network Models for Assessing the Role of Active Distribution Systems in Bulk Ancillary Services Markets," in *Power Systems Computation Conference*, Genoa, Italy, Jun. 2016.

[11] N. W. Miller, R.S. Zrebiec, R.W. Delmerico, and G. Hunt, "Design and Commissioning of a 5 MVA, 2.5 MWh Battery Energy Storage System," in *IEEE Transmission and Distribution Conference*, Los Angeles, CA, Sep. 1996.

[12] F. Lund, P. Sorensen, and J. Eek, „Reactive Power Capability of a Wind Turbine with Doubly Fed Induction Generator," in *Wind Energy*, vol. 10, pp. 379-394, Jul. 2007.

[13] G. K. Irungu, A. O. Akumu, and D. K. Murage, "Modeling Industrial Load Due to Severe Voltage Surges and Sags: 'A Case Study of Magadi Soda Company'," in *AFRICON 2007*, Windhoek, South Africa, Sep. 2007.

[14] M. Braun, "Provision of Ancillary Services by Distributed Generators," Ph.D. Dissertation, University of Kassel, Germany, 2008.

[15] Erlich, M. Wilch, and C.Feltes, "Reactive Power Generation by DFIG Based Wind Farms with AC Grid Connection," in *IEEE PowerTech*, Lausanne, Switzerland, Jun. 2008.

[16] *Power generation systems connected to the low-voltage distribution network*, Verband der Elektrotechnik Elektronik Informationstechnik e.V., VDE-AR-N 4105:2011-08, 2011.

[17] A. Ellis, et al., "Reactive Power Performance Requirements for Wind and Solar Plants," in *IEEE PES General Meeting*, San Diego, CA, Jul. 2012.

[18] S. Bolognani and S. Zampieri, "On the existence and linear approximation of the power flow solution in power distribution networks," in IEEE Transactions on Power Systems, vol. 31, no. 1, pp. 163-172, Jan. 2016.

[19] H. Kim and W. Kim, "Integrated Optimization of Combined Generation and Transmission Expansion Planning Considering Bus Voltage Limits," in *Journal of Electrical Engineering and Technology*, vol. 9, no. 4, pp. 1202-1209, Jul. 2014.

[20] Z. Yang, et al., "Optimal Power Flow Based on Successive Linear Approximation of Power Flow Equations," in *IET Generation, Transmission & Distribution*, vol. 10, no. 14, pp.3654-3662, Nov. 2016.